



# On the existence of a very metal-poor disc in the Milky Way

Hanyuan Zhang<sup>1</sup>  , Anke Ardern-Arentsen<sup>1</sup>  and Vasily Belokurov<sup>1</sup> 

<sup>1</sup> *Institute of Astronomy, University of Cambridge, Madingley Road, Cambridge CB3 0HA, UK*

12-16

arxiv:2311.09294v2

Reporter: Baokun Sun

# Outline

- 1. Introduction
- 2. Data
- 3. Chemo-Kinematic decomposition of the Milky Way
- 4. Discussion
- 5. Conclusions

# Introduction

- In the Milky Way (MW), **chemo-kinematic** analysis of ancient low-mass stars can provide strong, independent constraints on the emergence of the stellar disc. As precise stellar ages are not yet readily available for old stars, **stellar metallicity is routinely used instead as a proxy for a Galactic clock.**
- Multiple attempts to do so observationally agree that the MW's high- $\alpha$  disc stars with  **$[\text{Fe}/\text{H}] \lesssim -1$  have ages of  $\gtrsim 10$  Gyr.**
- The bulk of the stars at low metallicity, at least those accessible to observations currently, **likely formed elsewhere and were subsequently accreted onto the MW** – for example as part of the Gaia Sausage/Enceladus (GS/E) event and other, lower-mass mergers.

# Introduction

- Sestito et al. (2019, 2020) discussed three possible origins of the very metal-poor (VMP,  $[\text{Fe}/\text{H}] < -2.0$ ) disc-like/planar stars: (1) they formed in-situ in an early galactic disc; (2) they were born in the gas-rich building blocks of the proto-Milky Way, which formed the backbone of the later disc; (3) they are accreted from prograde minor mergers (after the disc is already in place).
- Finally, even if no net spin is present to begin with in the population of stars on halo-like orbits, over time, a prograde-retrograde asymmetry can be created by interactions with a rotating Galactic bar (e.g. Pérez-Villegas et al. 2017; Dillamore et al. 2023a). Dillamore et al. (2023a) show that a noticeable number of halo stars can get trapped in resonances with the growing or slowing down bar.

# XGBoost metallicity sample

- Andrae et al. (2023) derived stellar parameters of 175 million stars with Gaia DR3 XP spectra using the XGBoost algorithm. Their training sample consists of stars from APOGEE DR17 and an additional very/extremely metal-poor star sample from Li et al. (2022).
- Here, we only use their vetted bright ( $G < 16$ ) red-giant branch (RGB) star sample, which contains **17,558,141 stars** with high-confidence metallicity in the range from  $[M/H] \sim -3$  dex to beyond solar metallicity.

# Sample construction

- They manually introduce two further cuts by removing stars with  $E(B-V)_{\text{SFD}} > 0.5$  or  $|b| < 10^\circ$ , where  $E(B - V)$  is the colour excess from the **SFD dust map** Schlegel et al. (1998) queried using the dustmaps package (Green 2018).
- They use the photo-geometric distance provided by Bailer-Jones et al. (2021) instead of  $1/\text{parallax}$ . They select stars with  $\text{fpu} < 0.1$ .
- We performed numerical orbital integration for each star with a step-size of **1 Myr for 3 Gyr** using galpy (Bovy 2015).
- The maximum height above or below the disc plane,  $Z_{\text{max}}$ , and the orbital **eccentricity**,  $e$ , are subsequently obtained. The **energy**,  $E$ , of each orbit is also obtained using galpy. **The actions** ( $J_r$  for radial action,  $J_z$  for vertical action,  $J_\phi$  and (or  $L_z$ ) for azimuthal action) are calculated using Agama (Vasiliev 2019) with the Stäckel fudge method.

# Sample construction

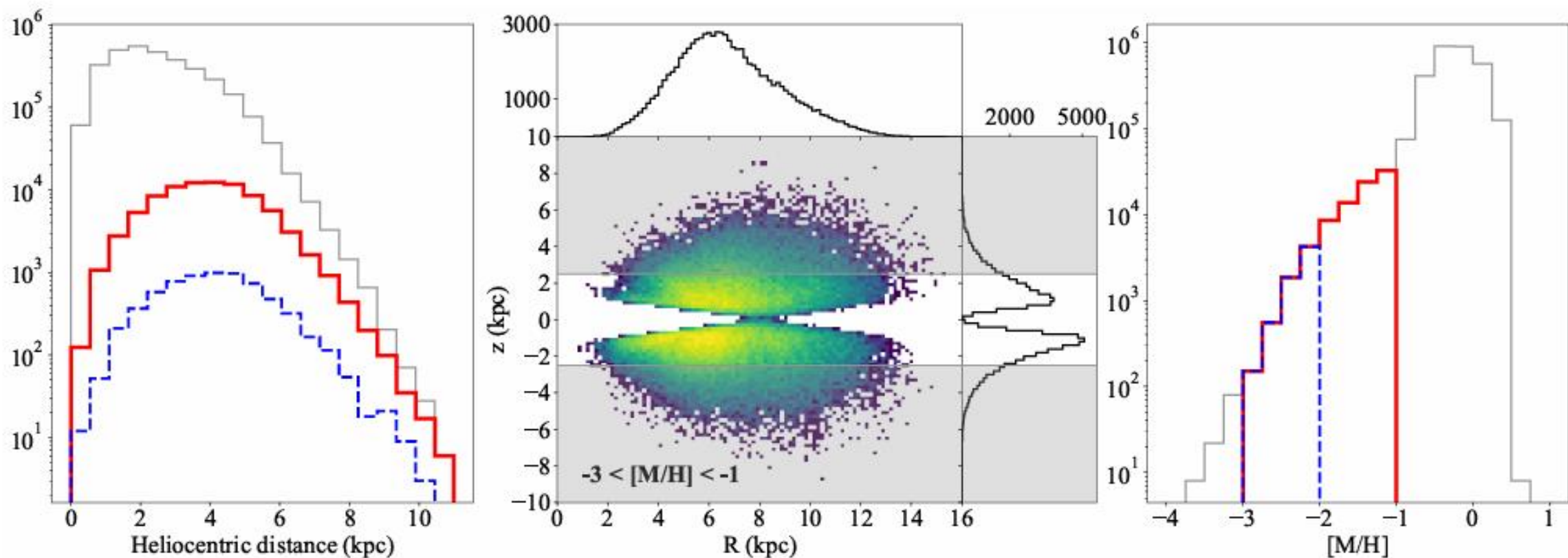


**Figure 1.** Properties of the final data sample after all selection cuts. Left: the heliocentric distance distribution. The solid red and dashed blue lines represent the distribution of stars with  $-3 < [M/H] < -1$  and  $-3 < [M/H] < -2$  respectively, while the grey line shows the distribution of the whole sample. Middle: the  $R - z$  distribution for stars with  $-3 < [M/H] < -1$ , in which the area at  $|z| > 2.5$  kpc is greyed out as we mainly focus on the analysis of stars with  $|z| < 2.5$  kpc. Right: metallicity distribution of our data sample. Line designation is the same as in the left panel.

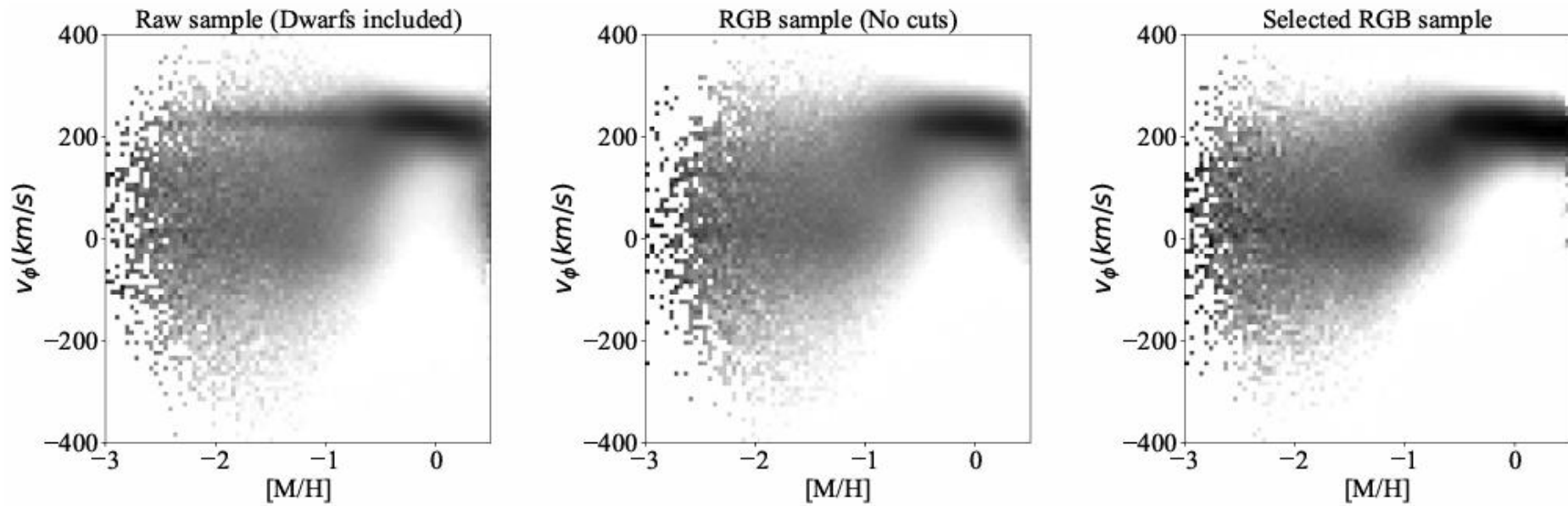


**Figure 2.** Column-normalised 2D histogram of stars in the  $[M/H]$ - $v_\phi$  plane. Left panel shows the raw sample that includes all stars in Andrae et al. (2023) without any cuts. A narrow band of fast-rotating stars can be seen extending into  $[M/H] < -1$ . This spurious signal is produced by hot stars with incorrectly assigned metallicities. Middle panel is for stars from the RGB sample with vetted metallicity in Andrae et al. (2023) before we further apply our selection cuts. To plot the left and middle panels, we randomly select stars from the sample so that the total number of stars is roughly the same as in our final sample. Right panel displays our final selected sample and reveals the sharp transition at  $[M/H] \sim -1.3$  that marks the spin-up phase of the Milky Way, intuitively corresponding to the epoch of the stellar disc formation.

The figure shows that there is a transition from **rotation-dominated orbits** (characterised by high azimuthal velocity  $V_\phi$  and low velocity dispersion) above  $[M/H] \sim -1.0$  to **pressure-supported orbits** (slow or zero rotation,  $v_\phi \approx 0$ , and high velocity dispersion) at lower metallicities ( $[M/H] < -1.0$ ).

Overall, at low metallicity, i.e.  $[M/H] < -1.5$ , there appears to be a systematic prevalence of **positive azimuthal velocities**, but the clear disc sequence ( $v_\phi \gtrsim 150$  km/s) does not extend below  $[M/H] \lesssim -1.3$ .

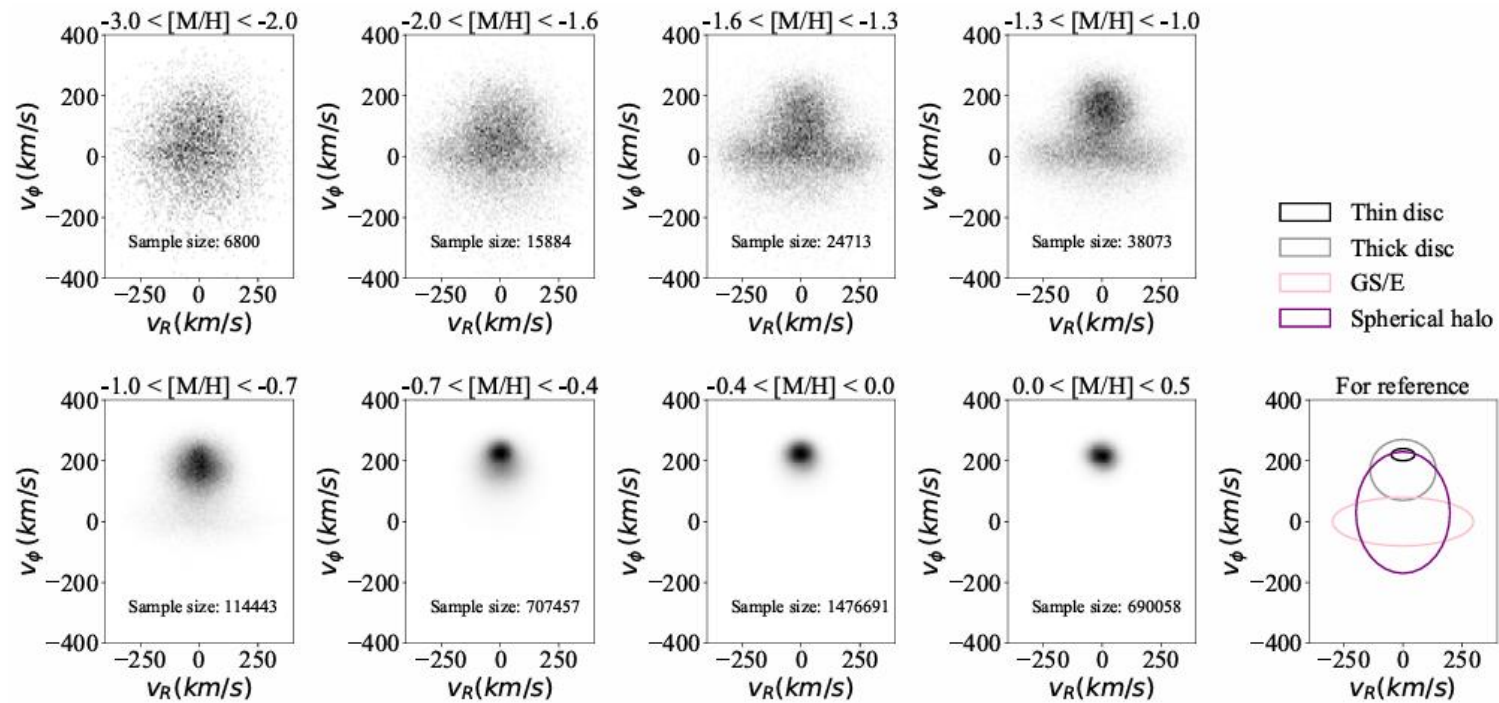


**Figure 3.** This shows the  $v_R$ - $v_\phi$  distribution for the sample in various metallicity bins, in which the sample size in each bin is noted in each panel. The lower right panel is drawn for reference, showing the expected location for several established Milky Way components, including two rotation-supported discs, the pressure-supported halo as well as the GS/E. The GS/E component is visible over a wide span of metallicity  $-2 < [M/H] < -0.7$  but its contribution at either end of this range is noticeably reduced. The velocity distribution is the broadest at  $[M/H] < -2$  and the narrowest at  $[M/H] > 0$ .

Fig.3 demonstrates that in the VMP regime ( $-3 < [M/H] < -2$ ), the velocity distribution is **halo-like**, i.e. approximately isotropic with little net rotation and without obvious disc-like features. Visually, the disc signature **disappears** in the metallicity bin of  $-2 < [M/H] \leq -1.6$ ; the thick disc quickly forms during the time corresponding to metallicities of  $-1.3 < [M/H] \leq -1$  and subsequently starts to dominate the sample in the next metallicity bin.

We do not attempt to fit GMMs to more metal-rich bins, partly because the distribution of the thin disc stars **deviates** significantly from a Gaussian-like distribution in  $v_R - v_\phi$  space.

We prefer the models with **fewer components** as the optimised fitting when BIC values are similar because they have a more straightforward physical interpretation.

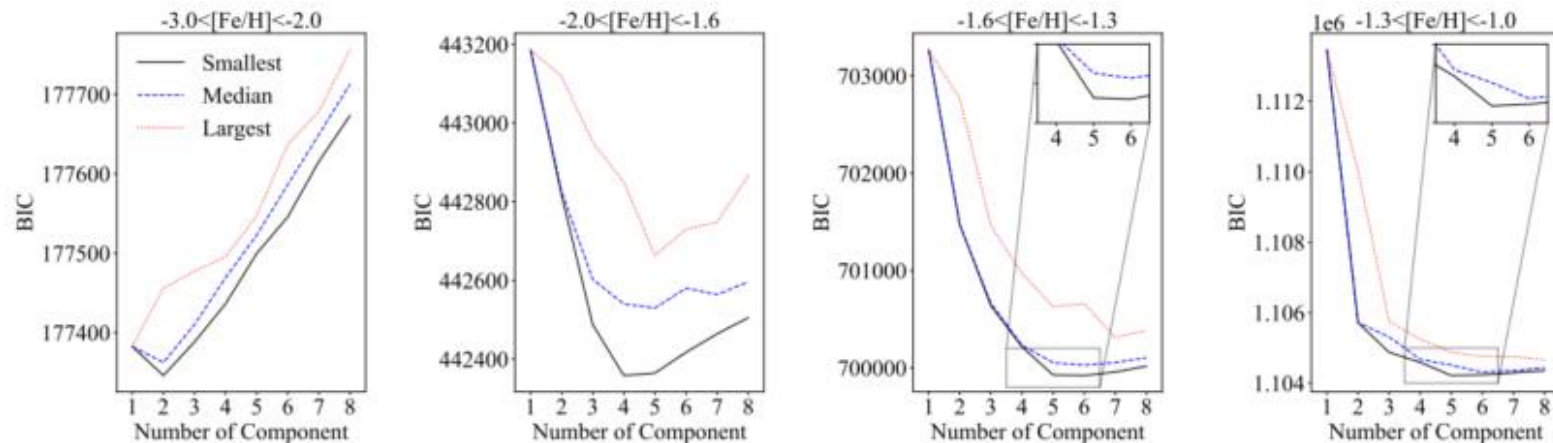


**Figure 4.** GMM's Bayesian information criteria (BIC) as a function of the number of model components in four metallicity bins between  $-3 < [M/H] < -1$ . In each  $[M/H]$  bin, we perform GMM fitting with different, random initial conditions 50 times, and the smallest, median, and largest BIC values are plotted in black-solid, blue-dashed, and red-dotted lines, respectively. The smallest BIC value indicates the optimum GMM fitting in that metallicity bin.

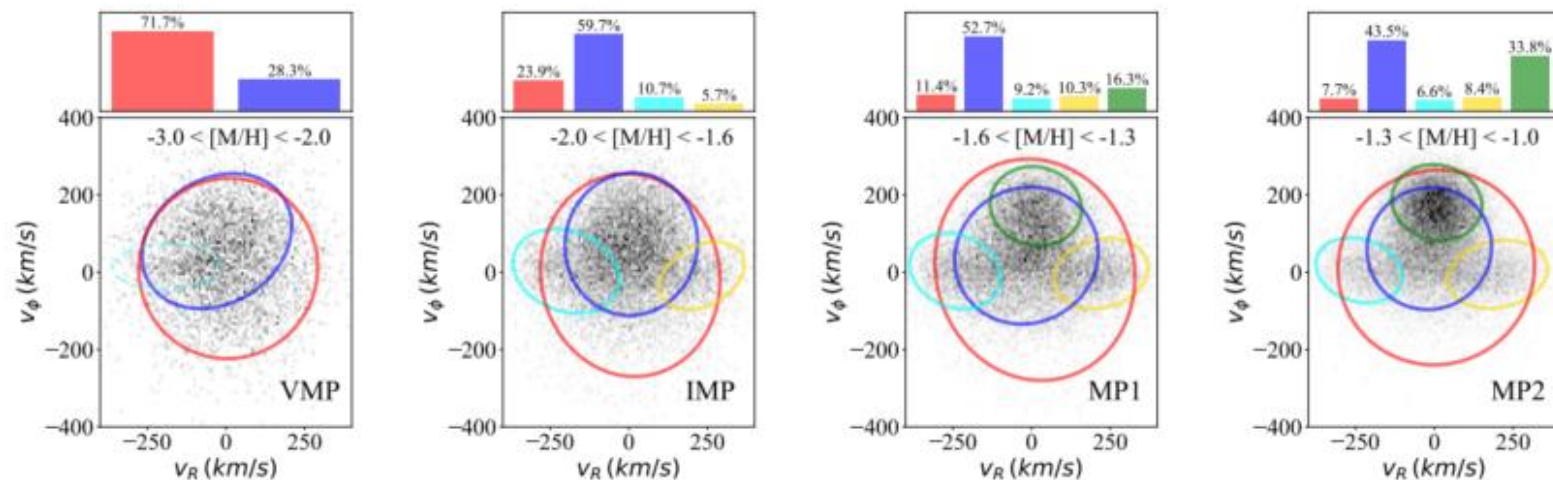


**Figure 5.** Optimum (as indicated by BIC) GMM for each metallicity bin, where each ellipse is the  $2\sigma$  contour of the corresponding model Gaussian for each sub-population. On the top of each panel, the histogram gives the fractional contribution for each identified substructure. Across  $[M/H]$  bins colour remains the same for Galactic components that are kinematically similar: red for the stationary halo, blue for the prograde halo, aqua and gold for GS/E components, and green for the rotation-supported disc. In the leftmost panel, the VMP bin, the aqua-dashed ellipse is not shown as the corresponding component is not identified in the optimum two-component GMM model, but it is recognised in the three-component GMM fit. The possible existence of this minor substructure can explain the tilting of the blue ellipse in the VMP regime and the asymmetry of the GS/E components in the IMP bin.

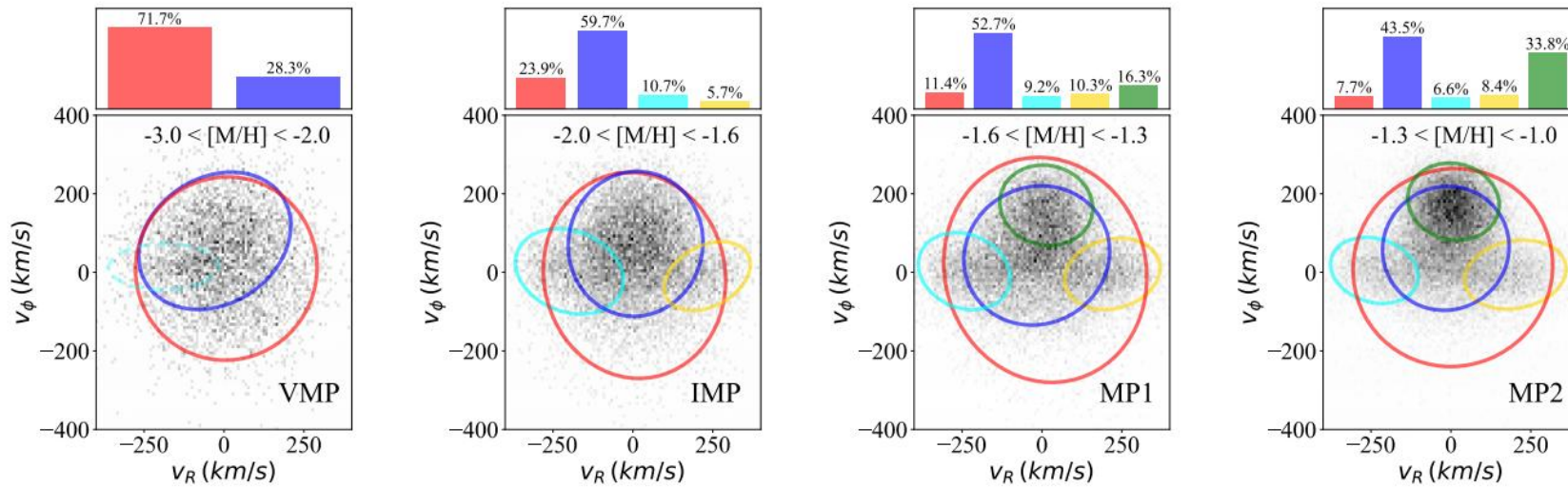


**Figure 5.** Optimum (as indicated by BIC) GMM for each metallicity bin, where each ellipse is the  $2\sigma$  contour of the corresponding model Gaussian for each sub-population. On the top of each panel, the histogram gives the fractional contribution for each identified substructure. Across  $[M/H]$  bins colour remains the same for Galactic components that are kinematically similar: red for the stationary halo, blue for the prograde halo, aqua and gold for GS/E components, and green for the rotation-supported disc. In the leftmost panel, the VMP bin, the aqua-dashed ellipse is not shown as the corresponding component is not identified in the optimum two-component GMM model, but it is recognised in the three-component GMM fit. The possible existence of this minor substructure can explain the tilting of the blue ellipse in the VMP regime and the asymmetry of the GS/E components in the IMP bin.

One of the components (red ellipse) does not have a significant net rotation ( $v_\phi \approx 0$  km/s) and a high velocity dispersion, hereafter we will refer to this as the stationary halo.

The other (blue ellipse) has a net positive rotational velocity  $v_\phi \approx 80$  km/s, and lower dispersion in  $v_\phi$  – hereafter we will refer to this as the prograde halo.

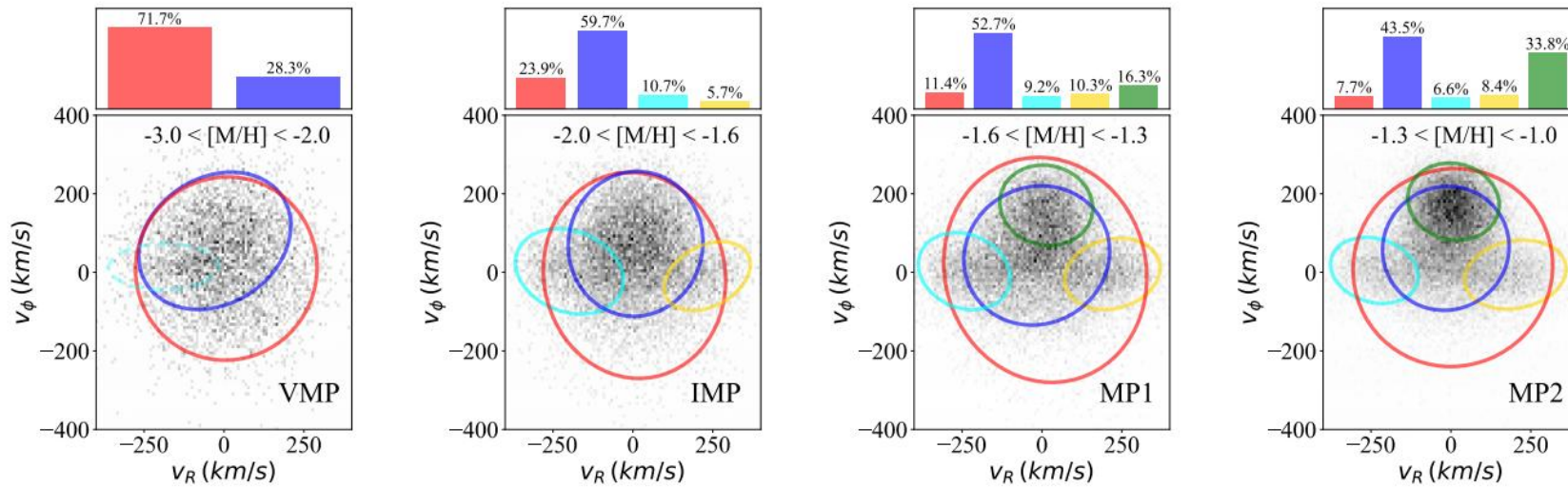


**Figure 5.** Optimum (as indicated by BIC) GMM for each metallicity bin, where each ellipse is the  $2\sigma$  contour of the corresponding model Gaussian for each sub-population. On the top of each panel, the histogram gives the fractional contribution for each identified substructure. Across  $[M/H]$  bins colour remains the same for Galactic components that are kinematically similar: red for the stationary halo, blue for the prograde halo, aqua and gold for GS/E components, and green for the rotation-supported disc. In the leftmost panel, the VMP bin, the aqua-dashed ellipse is not shown as the corresponding component is not identified in the optimum two-component GMM model, but it is recognised in the three-component GMM fit. The possible existence of this minor substructure can explain the tilting of the blue ellipse in the VMP regime and the asymmetry of the GS/E components in the IMP bin.

The GMM finds the same two halo components in the IMP bin, although the prograde halo now has more than 2.5x as many stars as the stationary halo, plus two additional sub-populations dominated by radial motions (the orange and aqua ellipses). These have very similar kinematics in  $v_\phi$  and  $v_z$ , but are **opposite in  $v_R$** , and are also found in the MP1 and MP2 bins. This kinematic signature suggests that they are likely connected to **GS/E**.

No rotation-supported structure is recognised by the GMM in the VMP and IMP bins, but a **rotation-supported**, disc-like population with  $V_{\text{rot}}/\sigma > 3$ , and  $v_{\phi} \sim 170$  km/s is found in the two MP bins ( $[M/H] > -1.6$ ). The weight factor for the disc population increases from 16.3% in the MP1 bin to 33.8% in the MP2 bin, consistent with rapid disc growth in this metallicity range.

The two components identified by the GMM for VMP stars (left panel in Fig. 5) both have **velocity dispersions larger than their mean velocities**, hinting at their halo-like nature.

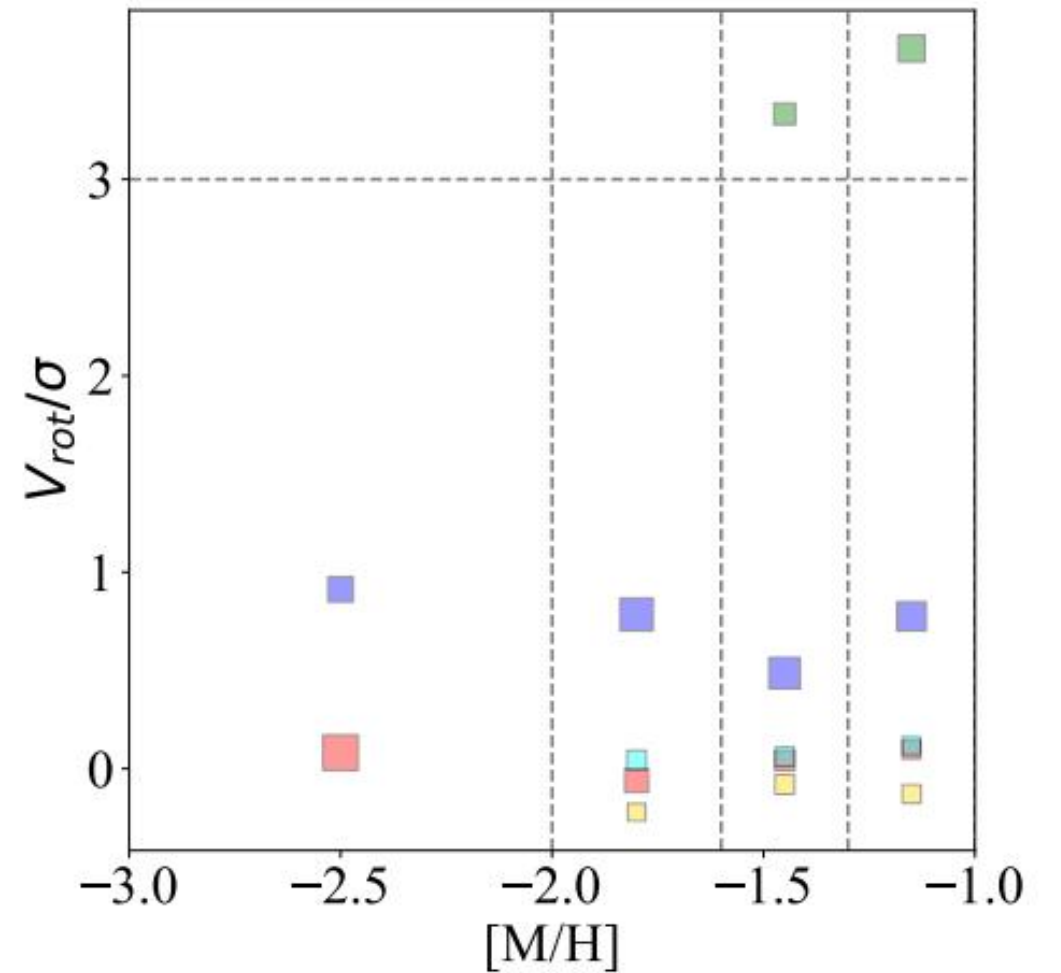


**Figure 6.** The ratio of the mean rotation velocity over the velocity dispersion in the azimuthal direction,  $V/\sigma$  for individual Gaussian components identified in each metallicity bin. The colour-coding is the same as in Fig. 5. The size of the square represents the fractional contribution of each component. Horizontal dashed line at  $V/\sigma = 3$  shows the conventional boundary for the rotation-supported disc. The uncertainties are negligible, so they are not plotted in this diagram.

# GMM residuals and the possible disc star fraction for VMP and IMP stars

We generate the same number of **mock stars** as the number of observed stars we have in each metallicity bin, where for each star, we generate  $v_R$ ,  $v_\phi$ , and  $v_z$  from the Gaussian distributions according to the parameters of the best-fit GMM model.

By comparing the observed disc residual and the mock disc tests, we conclude that the fraction of the disc population in the VMP regime of our sample must be in the range of **0 to 3%** (and **0 to 2%** in the IMP range).

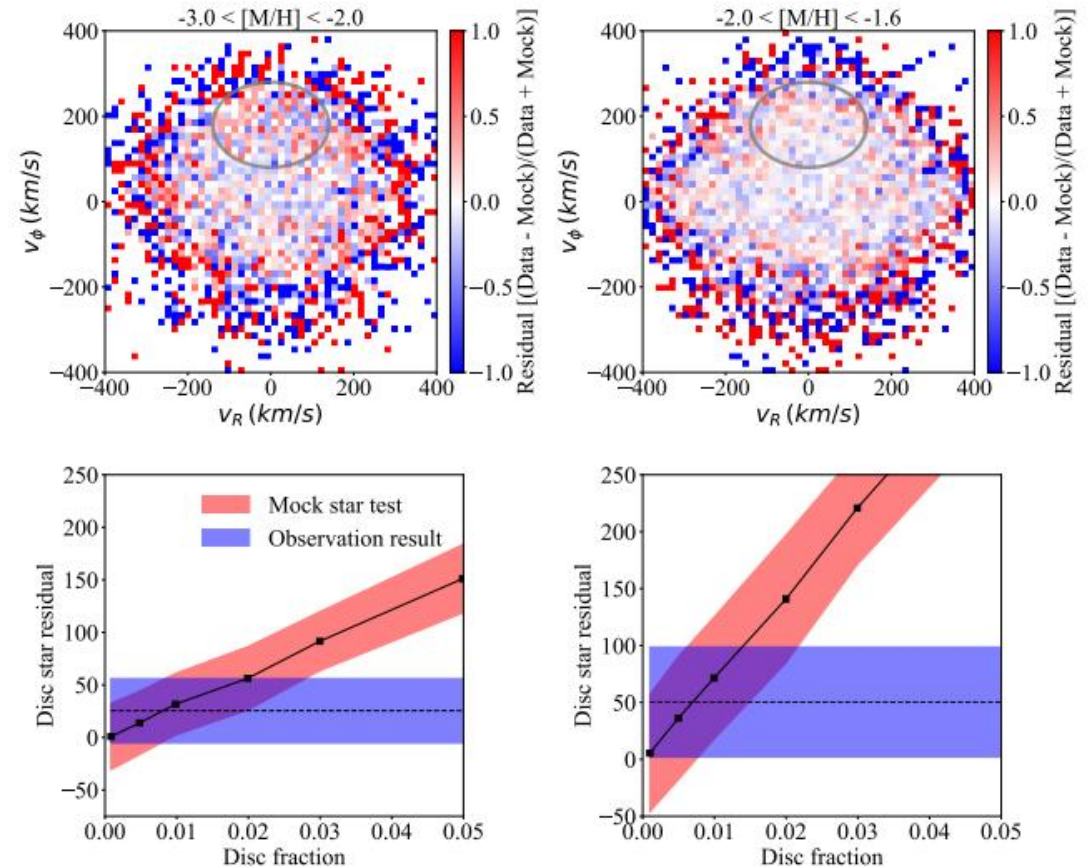


**Figure 7.** Top row gives the distribution of normalised residuals between the GMM and the data in the VMP (left) and IMP (right) bins. The normalised residual is defined as the number of mock stars subtracted from the number of observed stars divided by the sum of the observed and mock stars in each cell. The lack of strong systematic patterns, the low-amplitude and the small scatter of the residuals in the central regions verifies the validity of the GMM fit. The scatter in the periphery is larger due to random error. The grey ellipse indicates the region where stars with disc kinematics are expected in the  $v_R - v_\phi$  plane. The lower panels illustrate the expected disc residual as a function of the disc fraction in the samples obtained using mock star tests. In the bottom row, the blue-shaded region denotes the  $1\sigma$  uncertainty of the disc residual count computed using the Monte Carlo method. The solid black line and the red-shaded region show the residual and uncertainty of the mock sample (with manually added disc stars).

The two halo components dominate the metal-poor end. The **stationary halo** is the most significant component for  $[M/H] < -2.0$  and decreases in significance with increasing metallicity, while the **prograde halo** is the most dominant component for  $-2.0 < [M/H] < -1.0$ , at a constant level of fractional contribution. The **GS/E** contribution peaks around  $[M/H] = -1.5$ . The **disc population** is sub-dominant at low metallicity but appears around  $[M/H] \sim -1.6$  and becomes the main population by a factor of a few above  $[M/H] > -1.0$ .

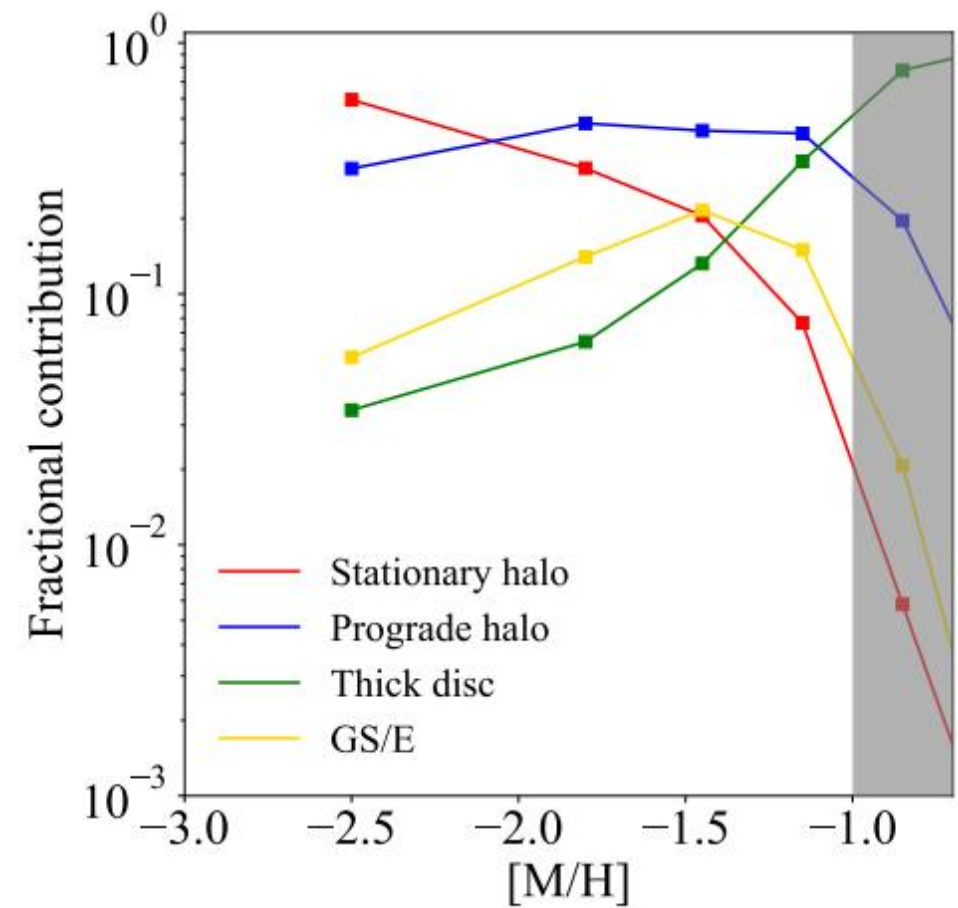


**Figure 8.** Fractional contribution of individual GMM components as a function of metallicity. The fractions are computed by freezing the mean and the covariance of each Gaussian in all metallicity bins and optimising for the weights only. We fix the GMM components according to the right panel in Fig. 5. The contributions from two GS/E components are added together. The metal-rich region ( $[M/H] > -1$ ) is shaded as we focus the discussion on lower metallicities  $[M/H] \leq -1$ . Note that the thick disc contribution dips quickly below  $\sim 10\%$  around  $[M/H] \sim -1.5$  and remains low. The fractional contribution of the prograde halo is constant for  $-2 < [M/H] < -1.3$  but is reduced at  $[M/H] < -2$  where the stationary halo's weight starts to dominate.

These distributions are lopsided towards high eccentricity,  $e > 0.5$  in all metal-poor bins. Only the most metal-rich bin considered,  $-1.3 < [M/H] < -1$  (red), exhibits the prevalence of orbits with  $e < 0.5$ . Combined with the qualitative arguments above, this further supports the earlier claims that in the Milky Way,  $[M/H] \sim -1.3$  is the lowest metallicity where an intact, rotation-supported disc can be detected.

They define the circularity as  $L_z / (r_{cicr} v_{cicr})$ , with  $r_{cicr}$  the circular velocity at galactocentric radius  $r$ . They adopt circularity  $> 0.7$  to assign stars to the cold disc, and assign stars with  $0.5 < \text{circularity} < 0.7$  and  $3.5 < R < 6 \times \text{Disc Scale Length}$  (for the Milky Way that roughly corresponds to  $3.5 < R < 13$  kpc) to the warm disc.

Quantitatively, 24 percent of VMP stars and 25 percent of IMP stars are assigned to the disc (cold and warm), However, 21 percent of the mock halo population is assigned to the disc as well. Note that, by definition, there is no disc present in the latter sample.

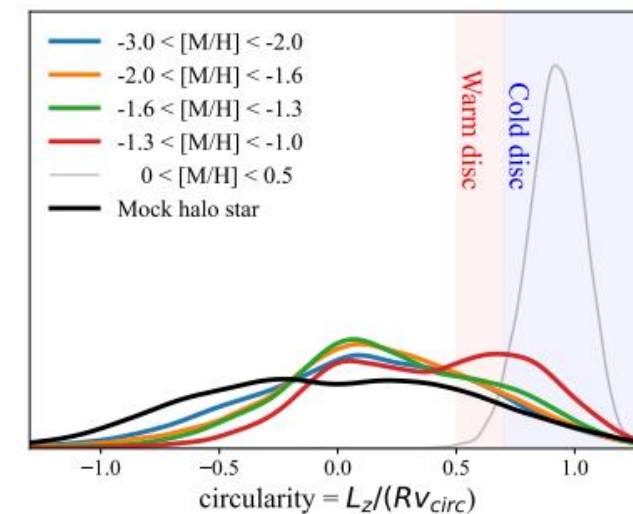
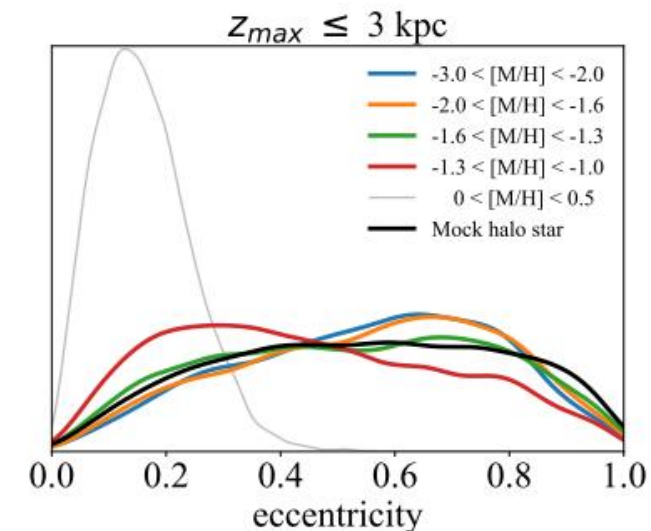
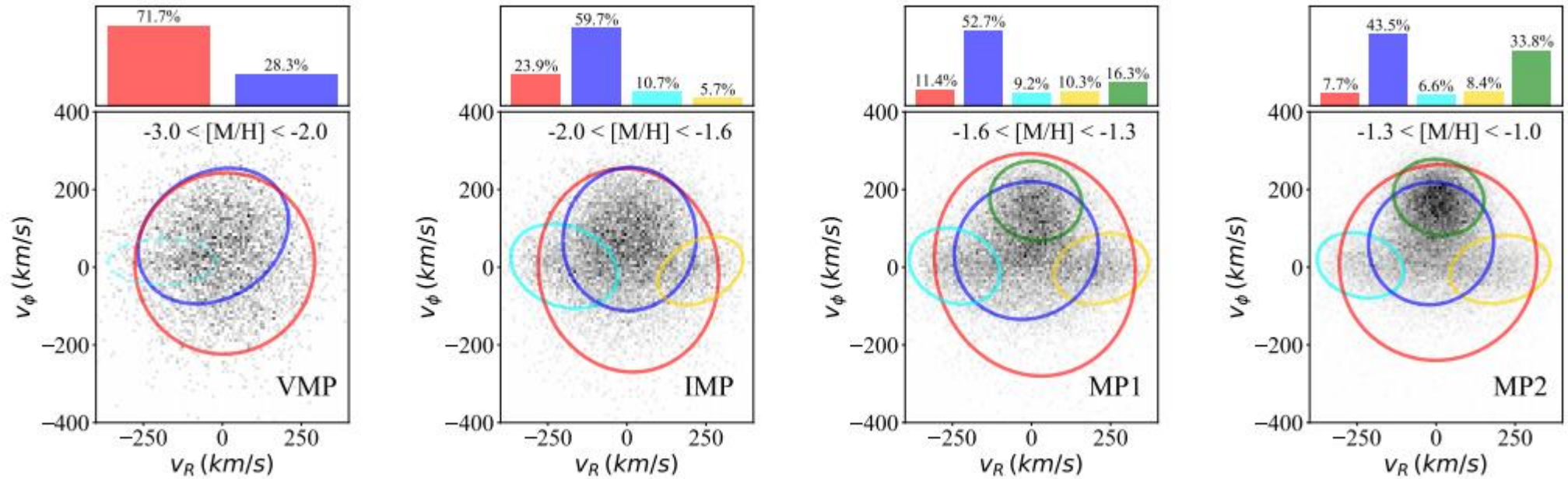


**Figure 10.** The eccentricity (top panel) and circularity (bottom panel) distributions of stars with  $-3 < [M/H] < -1$  in different metallicity bins (blue, orange, green, and red lines in order of increasing  $[M/H]$ ). Also shown are particles from a mock non-rotating halo population (thick black line). The mock particles are drawn from the isotropic NFW distribution function. The eccentricity distribution of metal-rich stars ( $0 < [M/H] < 0.5$ ) is also plotted in grey as a reference for the behaviour of a disc population. All distributions are computed using Kernel Density Estimation. The blue and red-shaded regions in the bottom panel are the cold and warm disc selection criteria defined in Sotillo-Ramos et al. (2023).



Circled by the dashed-aqua ellipse in the left panel of Fig. 5, a clear overdensity of stars with **high eccentricity** and **small net rotation** exist in the very metal-poor regime.

The possible causes of the overdensity are **recent accretion event debris** that is not fully phase-mixed, **bar-resonances** affecting halo stars, or the **selection function** (the latter is less likely).

# Conclusion

- In this work, we combine precise phase-space measurements from Gaia's astrometry and spectroscopy with a large sample of homogeneous metallicities derived from the low-resolution Gaia XP spectra, covering  $-3 < [M/H] < 0.5$ , to investigate the presence of a rotation-supported ( $v / \sigma > 1$ ) structure in the VMP ( $[M/H] < -2.0$ ) regime based on the 3D velocity distributions in various metallicity ranges.
- Fixing the GMM components to the combination of a stationary halo, a prograde halo, a thick disc and the GS/E, we show the transition from a dispersion-dominated to a disc-dominated Galaxy around  $[M/H] \approx -1.3$  (see Fig. 8).

# Conclusion

- The **prograde halo** component in our GMM analysis is the main culprit for the overdensity of prograde very metal-poor stars. This supports the conclusions from simulations that most very metal-poor stars were not born in the disc but originate from the time before the disc formed and/or were **accreted later on**.